# Detection and Recognition of Batteries on X-Ray Images of Waste Electrical and Electronic Equipment using Deep Learning

Wouter Sterkens [a,b], Dillam Diaz-Romero [a,b], Toon Goedemé [b], Wim Dewulf [a], Jef R. Peeters [a]

[a] Department of Mechanical Engineering – KU Leuven, 3001 Leuven, Belgium
[b] PSI-EAVISE – KU Leuven, 2860 Sint-Katelijne-Waver, Belgium

## Abstract

The trend of increased use of lithium-ion batteries, challenges the cost-effectiveness and safety of manual battery separation during the end-of-life treatment of Waste Electric and Electronic Equipment (WEEE). Therefore, the need for novel techniques to separate and sort batteries from WEEE is increasingly important. For this reason, the presented research investigates the potential to facilitate the development of novel techniques for battery extraction and sorting by examining the technical feasibility of predicting the presence, location, and type of batteries inside electronic devices with a deep learning object detection network using X-Ray images of the internal structure of WEEE. To determine the required X-ray imaging parameters, 532 electronic devices were arbitrarily collected from a recycling facility. From each product, two X-Ray Transmission (XRT) images were captured at two different X-Ray source configurations. Results obtained with the limited dataset are promising, demonstrating a 91% true positive rate and only a 6% false positive rate for classifying battery-containing devices. Moreover, a precision of 89% and a recall of 81% are demonstrated for battery detection, and an average precision of 85% and an average recall of 76% are demonstrated to distinguish amongst the following six battery technologies: cylindrical nickel-metal hydride or nickel-cadmium, cylindrical alkaline, cylindrical zinc-carbon, cylindrical lithium-ion, pouch lithium-ion, and button cell batteries. These results demonstrate the potential of using deep learning object detection on XRT-generated images for both automated battery extraction and sorting, regardless of the condition or shape of the products.

***Keywords:*** *Waste electrical and electronic equipment (WEEE); Battery sorting and recycling; X-Ray Transmission imaging; Deep learning computer vision; Object detection and recognition*

## 1. Introduction

### *1.1. EU policy in a transition towards a circular economy*

In the transition towards a circular economy, the European Union (EU) stands for both major opportunities and challenges, as highlighted in the ambitious circular economy action plan adopted by the European Commission (2020). The proposed strategies envisage additional savings of up to €600 billion for EU businesses, corresponding to 8% of their annual turnover and 450 million tonne reduction in EU carbon emissions by 2030 (European Commission, 2015). In this action plan the European Commission identifies the Electronics and ICT sector as one of the key value chains encompassing major opportunities. Besides improving the collection rate, the action plan highlights the need to improve existing waste management strategies, since the implementation of recycling and reuse is essential to accomplish better closed material loops (European Commission, 2020). The need for strategies to efficiently treat Waste Electrical and Electronic Equipment (WEEE) is vital, as many components in this waste stream contain both high fractions of critical raw materials (CRMs) and hazardous materials. CRMs have a high risk associated with their supply and are in high demand for the European manufacturing industry, while it is mandatory to treat components containing hazardous materials separately, according to the directive of the European Parliament and the European Council (2018).

The need for novel strategies to efficiently sort and separate batteries is particularly urgent, as batteries commonly contain both CRMs and hazardous materials. Examples of CRMs commonly present in batteries are cobalt and natural graphite in lithium-ion batteries (LIBs), antimony in lead-acid batteries, neodymium, praseodymium, lanthanum, and cerium in nickel-metal hydride batteries, and indium in alkaline batteries (Mathieux et al., 2017; Deloitte Sustainability et al., 2017; Umicore, 2020). Examples of hazardous materials commonly used in batteries are mercury, lead, and cadmium (Bigum et al., 2017). Therefore, it is also mandatory to separate all batteries from WEEE according to the WEEE Directive (2012, p. 26). Due to the popularity of portable devices, a substantial proportion of today's WEEE must already be sorted and dismantled for battery removal and this proportion is only expected to increase.

*1.2. Challenges of the current process to separate and sort batteries from WEEE*

Most batteries from WEEE can be found in the product categories of small domestic appliances, IT and telecommunications equipment (SDA and IT), which are often jointly collected. In addition to batteries, it is also mandatory to separately treat other components, such as printer cartridges and cathode ray tubes. In some cases, it might also be economically viable to manually dismantle components, such as printed wiring boards with high concentrations of precious metals (Peeters et al., 2016). Therefore, as shown in Figure 1, at the outset of a WEEE recycling line, specific products, such as printers, lamps, and laptops are first selected to be separately treated in dedicated recycling lines. At the same time, cables and components containing wood and glass are also separated and sorted. Afterwards, all products are sorted as either battery-containing or non-battery-containing based on manual inspection.

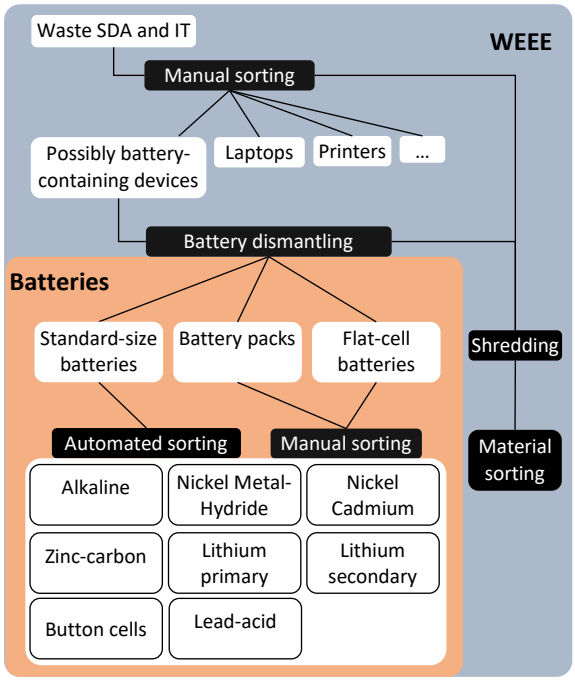


Figure 1. Summary of battery separation and sorting from Small Domestic Appliances, IT and telecommunications equipment

Thereafter, all battery-containing devices are manually dismantled to separate the batteries. This is a highly labour intensive procedure because all devices sorted as potentially battery-containing must be manually treated. A large Belgian recycling company also reported that an increasing share of batteries cannot be removed by unscrewing the product because they are glued or welded on to the product, or because the product is assembled using many snap-fits. Therefore, more time is lost opening and inspecting devices that do not (or no longer) contain a battery, as it is not evident to determine whether possibly battery-containing devices still contain batteries based on a visual inspection, and more time is required to manually remove the batteries. As a result, the labour intensity of dismantling batteries is expected to further increase in the near future.

To address the need for more cost-efficient dismantling, a setup to smash and break open devices using a rotating drum or an impact crusher could be considered in order to ease manual battery separation. However, in these systems batteries can be damaged because of the destructive manner of separation. Therefore, these

processes are not suitable for products containing LIBs, as the battery can be easily damaged and cause fires, or lead acid batteries, which can leak when damaged. Therefore, sorting the devices according to the battery type would be of great value for this approach. In addition, small products with rubber or thick casings, such as watches, card readers, and electric tools are likely not to break open and therefore would still require manual intervention. To avoid these hazards, the procedure could also be automated by first crushing the waste stream in an inert environment and then automatically sorting the batteries from the waste stream. However, sorting the potentially damaged batteries from other components in WEEE products will be challenging, as the physical properties of damaged batteries can be similar to other components, such as electric motors or metal casings, and because batteries are often not be fully liberated from the housing materials. Since such systems are not currently available, battery-containing products still need to be sorted first and then be redirected to a dismantling step.

After dismantling, factory workers sort the batteries into standard-sized cylindrical batteries, battery packs, and flat-cell battery designs, such as lithium-ion and lithium-polymer pouch cells from phones, as shown in Figure 1. The remainder of the dismantled devices are commonly shredded and sorted together with the non-battery-containing devices for material recycling under the condition that they no longer contain hazardous materials. Along with batteries from dedicated battery collection points, the dismantled standard-sized cylindrical batteries are then sorted into multiple groups based on their chemical content. This is done in a fully automated sorting process in which batteries are sorted based on their shape using sieving techniques, followed by sorting based on colour imaging, weight, electromagnetic resonance or X-Ray fluorescence (XRF) (Hedegor et al., 2004; Mallant et al., 1996; Redux, 2020; Refind, 2019). This allows the sorting of the batteries into eight different chemical families with a purity of up to 99.7% (Bebat, 2020). Due to their wide variation in shape, battery packs and flat-cell batteries cannot be handled with these automated techniques and to date are sorted manually.

Afterwards, the sorted groups of batteries and battery packs can be treated directly in pyrometallurgical, hydrometallurgical or hybrid processes (Cheret & Santen, 2007). However, in order to improve recovery efficiency, procedures have been developed to pre-recycle batteries and battery packs by disassembly (Herrmann et al., 2012; Sonoc et al., 2015), under-water explosion (Yamaji et al., 2011), ultrasonic washing (Li et al., 2009), or shredding (Gratz et al., 2014; Wang et al., 2016), followed by optical or XRF sorting of the materials themselves. As an alternative to improving the current methods to sort and dismantle batteries from WEEE, future studies might focus on directly implementing these destructive pre-recycling procedures to battery-containing WEEE in a continuous procedure instead (e.g. directly shredding battery-containing WEEE in an inert environment followed by size-based sorting of the materials). However, to the best of our knowledge, no studies have been conducted to date on technical feasibility, potential additional recovery losses, or sorting requirements prior to direct treatment.

Hence, the sorting of battery-containing products, the dismantling of batteries, and the sorting of dismantled batteries requires multiple steps and is laborious to this day, resulting in high treatment costs. These treatment costs are expected to increase in the coming years because of the following reasons: (1) the share of product-containing batteries is expected to increase drastically, (2) the share of flat-cell battery types is expected to grow, (3) the battery dismantling time is expected to increase and (4) the cost of manual labour is expected to rise, especially in Belgium, as tax reductions given to protected working environments, which are widely adopted in the resource management sector, have been significantly reduced by recent legislative changes (Flemish Department of Work and Social Economy, 2013). In addition, there remains a risk of exposure to hazardous substances during manual sorting and dismantling. Furthermore, because of the rise of LIBs in WEEE, which can heat up rapidly when short-circuited or perforated, an increasing number of fire accidents have been reported in recycling facilities (Lisbona & Snee, 2011). Since the number of LIBs in WEEE is only expected to increase, such

fire hazards are also expected to increase. For all these reasons, there is an urgent need for more cost-efficient systems to sort and separate batteries from WEEE.

### *1.3. Deep learning for waste sorting*

To the best of the authors' knowledge, no automated systems to sort battery-containing products from non-battery-containing products, to detect the location of batteries inside of WEEE, or to sort battery packs and flat-cell battery types based on their chemical content exists to date. Nonetheless, recent developments in deep learning architectures for computer vision have drastically improved the ability to detect and recognise objects on images. These architectures consist of a series of layers which, in combination with activation function, identify characteristics that are increasingly distinctive as one layer passes information to the next. Resulting from these advancements, the ability of state-of-the-art deep learning methodologies to accurately sort waste has improved drastically in the recent years. Classification setups have been developed to sort and recycle a broad range of recycling applications, such as construction waste, cardboard and plastics (*AMP Cortex*$^{TM}$, 2020; *Max-AI*, 2020; Bobulski & Kubanek, 2019; Lukka et al., 2014). In the field of WEEE recycling, IDlab, a research group at the University of Antwerp, has managed to successfully categorise WEEE into product groups, such as SDA, IT, large household devices, and small household devices with a proclaimed accuracy of more than 90% by making use of a deep learning architecture and a large dataset of more than one million images of WEEE which was acquired in collaboration with the Belgian recycling association Recupel (Recupel, 2019). In collaboration with the Danish Institute of Technology (DTI), the Swedish company Refind has also demonstrated the feasibility of sorting different types of cell-phones, printed circuit boards, mixed electronic scrap, and also batteries by capturing colour images and applying a deep learning architecture (Danish Technological Institute (DTI) et al., 2018; Refind, 2019). Similarly, Karbasi *et al.* performed a study to sort different types of coin cells (Karbasi et al., 2018).

However all the methods adopted in previous research rely on images portraying the outer shape of the materials or products. Hence, dirt and outer damage, commonly encountered in WEEE, can strongly affect detection accuracies. Additionally, only determining the product category or model is insufficient to verify the presence of batteries or other components, and can never be used to determine location or type of batteries within products. As a result, deep learning architectures trained for detection and classification in colour images can and are today only used to sort standard batteries after they have been dismantled (Recupel, 2019; Refind, 2019).

### *1.4. Applying deep learning to XRT images*

For other applications where the inner features of objects need to be evaluated, such as baggage screening, food processing, and medical imaging, X-Ray Transmission (XRT) imaging is commonly adopted. In these fields, deep learning object detection on XRT images has been applied, for example, to detect Pneumonia on chest X-Ray images (Rajpurkar et al., 2017) and detect prohibited products on luggage X-Ray images (Akcay et al., 2018). XRT is a 2D imaging technique in which the inspected object is bombarded with an X-Ray beam and the local amount of X-Ray attenuation, being the reduction in X-Ray intensity as it traverses a sample, is measured pixel-wise with a detector. The amount of local attenuation depends on variables, such as material density and thickness. Therefore, XRT imaging allows the creation of an image of the internal structure of the product. This is in contrast with X-Ray fluorescence (XRF) that also bombards the material with an X-Ray beam and analyses the wavelengths of the fluorescence, which provides information on the actual elemental composition, but which can only be used for surface analysis. Hence, XRF can only be used to define the battery type after opening the batteries, while XRT can analyse the batteries while still inside an electronic product. For waste recycling, XRT has

previously been adopted to identify organic and inorganic waste, sort plastics and sort metals (InnospeXion, 2020; Montagner et al., 2014; Takezawa et al., 2015). Tests have also been performed to determine the degradation of LIBs by evaluating the state of battery features visible on XRT images (Chen & Shen, 2017). Specifically for inspecting untreated WEEE, there are significant benefits to XRT imaging prior to sorting and treatment. One of the benefits is that dirt on and damage to the product housing will not affect the detection and recognition of components inside of the device with deep learning architectures. The exterior shape of products also varies dramatically between different makes and models, whereas the same components are often used for various products. As a result, there is significantly less variation in internal component shapes in XRT images compared to the variation in product shapes in colour images, which will also be of great benefit to the detection accuracy of deep learning architectures applied to XRT images.

As there is an urgent need for new strategies to more accurately detect and classify batteries in WEEE in a more economically viable and safe manner, the presented research investigates the possibility (1) to detect the presence or absence of batteries to improve the sorting of battery-containing devices, (2) to determine the location of the batteries inside of the product to ease manual or even enable automated battery removal, and (3) to recognize the battery-structure in order to determine the battery type and sort batteries into groups based on their chemistry to recycle raw materials when the batteries are removed.

## 2. Materials and methods

### *2.1. Machine settings for X-Ray Transmission*

For this study, a Nikon XT H 225 ST CT-scanner was used to capture single X-Ray images of WEEE. Tungsten was selected as target material to generate high-intensity X-rays with a 0.5mm copper filter to reduce the amount of low-intensity X-Rays, and thus reduce the effect of underestimating material thickness and increase the ability to distinguish features by examining intensity differences. The used configuration captures images with a flat table to mount objects in the centre, the X-Ray source on one side and the detector on the other side. Thus, when an object is placed on the table without support, a side-view X-Ray image is captured. To examine the internal structure of WEEE, a top-view X-Ray image is generally desired instead, because a top-view image of one of the object's natural resting planes often displays the most visible features. For example, a side-view X-Ray image of a cell phone or a laptop is less desirable than a top-view X-Ray image. To mimic this condition, the products were placed upright in the CT-scanner by using a polystyrene bracket, as shown in Figure 2.

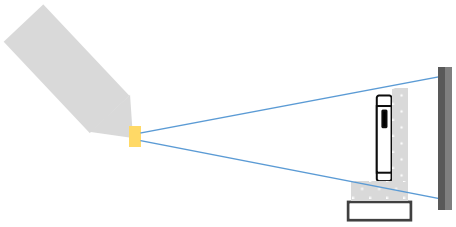

Figure 2. Side-view sketch of the CT-scanner setup

In an industrial sorting line, X-ray images could be similarly generated by using an X-ray line-scanner in combination with a conveyor belt, similar systems used for X-Ray baggage screening. One of the main parameters influencing the production cost of such a system is the required power to generate the maximum tube voltage and current, as increasing the current results in a larger amount of released electrons from a heated filament in a vacuum tube, which consequently results in a higher amount of generated X-Rays. Increasing the voltage

amplifies the acceleration of the electrons, which in turn results in greater penetration of the photons into the sample. Hence, the cost of the system will increase significantly, not only for the XRT-imaging equipment, but also because more stringent safety measures must be implemented, which can account for up to half of the production cost of an XRT machine.

Thereafter, the minimal power required was determined to be able to firstly, visually distinguish the battery from other components, and secondly, visually distinguish different types of batteries from each other. A small dataset of X-Ray images of battery-containing electronic devices at different voltages and currents was captured in steps of 20 ranging from 40kV to 180kV and 20µA to 140µA with an exposure time of 1,415s. Because casings of small domestic appliances mostly consist of plastic or thin-metal casings, they can be penetrated by relatively low-intensity X-Ray beams. As a result, batteries could already be detected visually on images generated at 60kV and 40µA, which is attainable by regular X-Ray devices for industrial inspection. However, the contrasting anode-cathode layers and other dense structural features of many battery types required more penetration to be easily visually distinguishable, resulting in a higher voltage and current requirement of 120kV and 100µA for visual battery-type recognition. An even higher voltage and current were determined not to be desired, as battery technologies with less dense materials, such as LIB pouch cells and zinc-carbon batteries, would saturate, and as a result be less visible in the X-Ray image.

### *2.2. Collection and annotation of datasets*

To train a neural network and evaluate the performance of battery detection and battery-structure recognition, 546 electronic devices, sorted by factory workers as possibly battery-containing, were arbitrarily picked from a conveyor at a Belgian WEEE recycling facility. The collected devices were first categorised according to the type of product. Device categories with five or more devices are shown in Table 1.

Table 1. Product categories with more than five devices in the dataset.

| Number of devices per category | | | | | | | | | | | | | | | | | | | | | |
|---|---|---|---|---|---|---|---|---|---|---|---|---|---|---|---|---|---|---|---|---|---|
| Toy | Remote Control | Mobile Phone | Flashlight | Calculator | Cordless Telephone | Garden Solar Lamp | Bank Terminal | Watch | Toothbrush | Digital Camera | Electric Razor | Drill | Vacuum Cleaner | MP3 player | Walkie-Talkie | Display | Portable Speaker | Powerbank | DVD player | Film Camera | Mini Flashlight | Scale | Tablet |
| 58 | 45 | 45 | 26 | 26 | 26 | 25 | 25 | 20 | 18 | 16 | 15 | 14 | 13 | 10 | 10 | 10 | 8 | 7 | 7 | 7 | 6 | 5 | 5 |

Subsequently, X-ray images of all devices were captured with the CT-scanner setup. Both at the source settings intended for battery detection and battery structure recognition, resulting in two image datasets. For battery detection, all batteries were manually annotated by drawing a rectangular, non-rotated bounding box around the circumference of every battery. This was done on the set of X-Ray images captured for battery-structure recognition, as it provided the most detail. To prevent the annotation of components similar to batteries, X-Ray images of batteries were first captured for reference. When the references remained insufficient, the device was opened for verification. For the goal of recognizing different types of batteries, the annotations were also classified according to their battery structure, and the devices were also opened if the type could not be visually verified. Fourteen devices were excluded from the dataset for both the evaluation for battery detection and battery recognition, as they contained a type of battery-structure with fewer than 10 instances present in the whole dataset. This was determined to be insufficient to train a network to recognize those battery structures. Examples of excluded products were four handheld vacuum cleaners containing a lead-acid battery pack and two lithium-polymer power banks.

This resulted in a product dataset of 532 devices containing 943 batteries (often multiple batteries per product). 498 devices contained at least one battery and the annotations for battery structure recognition consisted of six classes of battery-structures: cylindrical nickel-metal hydride (NiMH) or nickel-cadmium (NiCd), alkaline, zinc-carbon and lithium-ion batteries, pouch lithium-ion batteries, and button cells. An example image of each class, both at high and low XRT power settings, is shown in Figure 3, along with the associated battery shape and collection group.

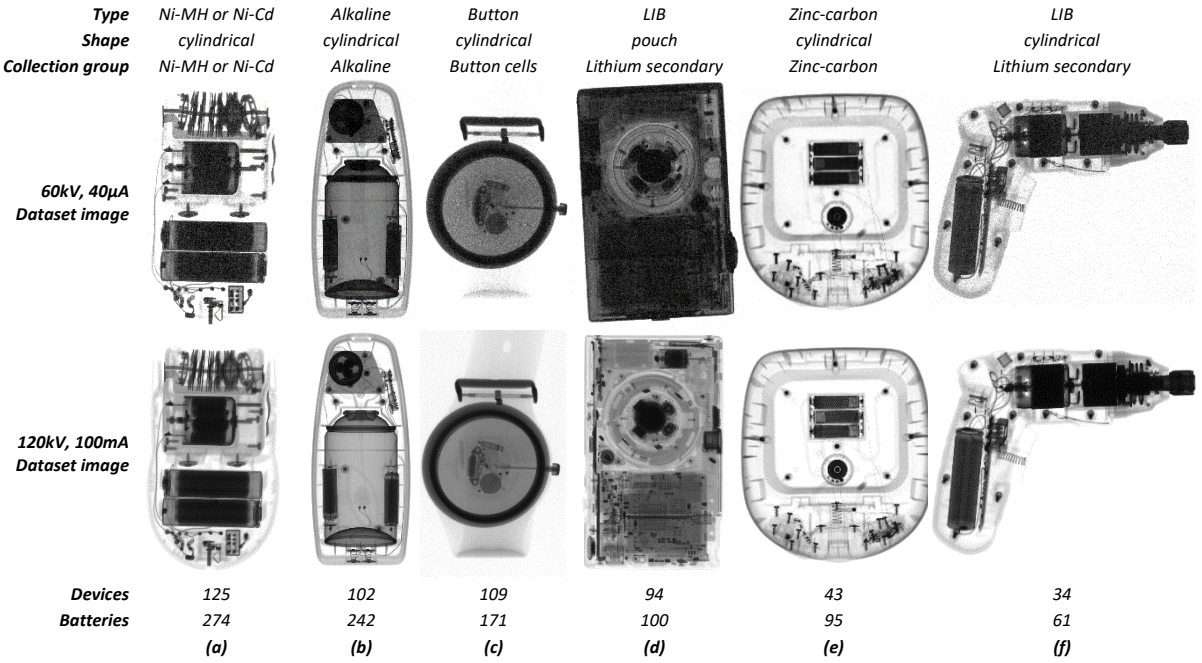


Figure 3. Example X-Ray images of devices at high and low power X-Ray settings with the number of devices and batteries given for each class: (a) cylindrical nickel-metal hydride (NiMH) or nickel-cadmium (NiCd), (b) cylindrical alkaline, (c) button cells, (d) pouch lithium-ion, (e) cylindrical zinc-carbon and (f) cylindrical lithium-ion.

NiMH and NiCd batteries were annotated as a single class, as these batteries hardly differ in structure. However, it should be noted that NiMH and NiCd batteries are treated separately, which would require an additional sorting step prior to material recycling, for example, based on weight and electromagnetic resonance. Button cells are also considered as a single class, whereas the design and chemical composition of these batteries can significantly vary from lithium primary to silver-oxide to zinc-air. Nonetheless, button cells are often recycled as one group and the number of button cells in this dataset was limited. By annotating all button cells as one class, the class size was also increased and the difference in the number of samples between classes was reduced. This resulted in less class imbalance during training and a reduced chance of poor recognition results on classes with few images.

### *2.3. Dataset training and evaluation*

To evaluate the performance of classifying battery-containing devices, detecting batteries, and recognizing battery-structures, the deep learning single-stage architecture YOLOv2 was implemented (Redmon & Farhadi, 2016). Unlike two-stage architectures, such as Faster R-CNN (Ren et al., 2016), one-stage detection networks perform both object detection and recognition in a unified regression procedure, resulting in faster training and

prediction speeds. In the past, this used to come at the cost of lower localization accuracies, but with the adoption of fine-grained features to improve the localization of smaller objects and by directly detecting the centre of objects, the average localization accuracies of YOLOv2 are on par with two-stage architectures (Jiao et al., 2019). YOLOv2 was selected over other single-stage architectures, such as SSD (Liu et al., 2016), DSSD (Fu et al., 2017) and RetinaNet (Lin et al., 2017), because previous research has shown that YOLOV2 can achieve real-time prediction speeds with competitive detection accuracies and fast training speeds (Jiao et al., 2019). However, a larger selection of state-of-the-art architectures, including novel developments on the YOLO architecture, will be investigated for the envisaged application in future work.

To prepare the high and low power X-Ray image datasets, both image datasets of the 498 battery-containing devices were divided equally into 80% for training and 20% for evaluation. The 34 devices that did not contain a battery were also added to the evaluation set, resulting in 398 devices for training and 132 devices for validation. Weights pre-trained on ImageNet, which is a large database of images, were used to have existing natural-image filters as a starting point for the trainings performed in this research (Russakovsky et al., 2015). Before training, the images were cropped to the shape of the device and additionally cropped and flipped randomly to increase variation and a total amount of 115 000 batch-iterations of 64 images were performed on a NVidia Tesla V100 GPU using the Lightnet framework (Ophoff, 2018). The network size was deliberately set to be 448x448, and randomly reshaped between 320x320 and 608x608 every 10 batch-iterations, even though the original image resolution was 2000x2000. A small network size was used to achieve high detection speeds and to train the network on a resolution that is more realistic for an inline XRT line scanner as commonly used in industrial applications.

First, the network was trained to detect batteries on both the low and high intensity X-Ray image datasets. Although, all batteries were visually detectable on the low intensity X-Ray image dataset, the possibility to further improve the ability to detect batteries on higher-intensity X-Ray images with more available features was evaluated in this manner. The trained weights were not only used to evaluate the ability to detect the location of batteries inside of the device, but also to distinguish battery-containing devices from non-battery-containing devices in which not a single battery is present. Thereafter, the network was trained to recognize the different battery structures on both the low and high power X-Ray image datasets by making use of the battery structure annotations (six classes). In this manner, the ability to perform battery recognition with relatively low- and high powered X-Rays was evaluated.

## 3. Results and discussion

### *3.1. Classification of battery-containing devices for sorting*

Using trained weights to detect batteries in the validation image set, a number of battery locations are predicted for each image with a certain detection confidence for each location. To evaluate the performance of this methodology for classification, the receiver operator characteristic (ROC) curve was calculated. The ROC-curve is determined by calculating the true positive rate (TPR), which is also called recall or *probability of detection*, against the false positive rate (FPR) which is also called the *probability of false alarm* at multiple confidence thresholds. The TPR and the FPR are defined as follows:

$$\mathrm{TPR} = \frac{\text{true positives}}{\text{true positives} + \text{false negatives}} \tag{1}$$

$$\mathrm{FPR} = \frac{\text{false positives}}{\text{false positives} + \text{true negatives}} \tag{2}$$

An image classification is counted as a positive when any number of batteries are detected (battery-containing) and as a negative when no single battery is detected (non-battery-containing). The prediction is counted as true or false compared to the ground truth. For example, when one or more batteries are detected on an image of a non-battery-containing device, the prediction is false, and thus the image classification is counted as a false positive. The calculated ROC-curve is shown in Figure 4.

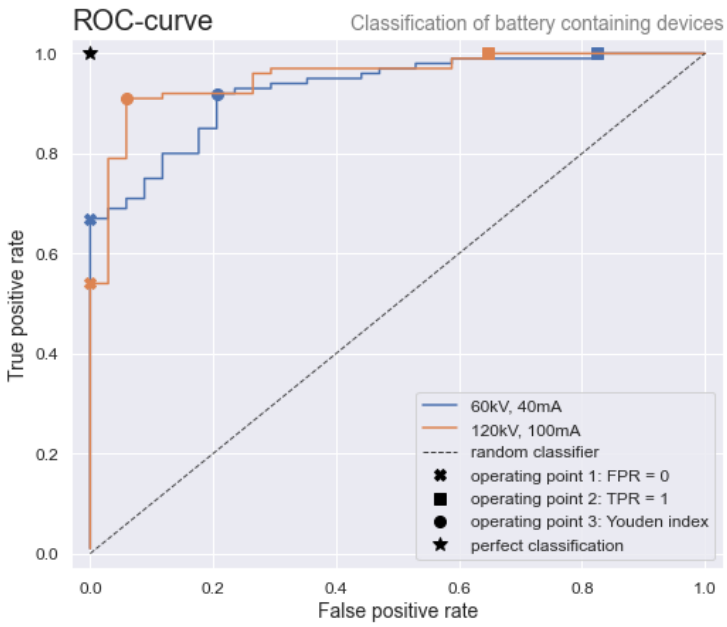


Figure 4. ROC-curve of classifying battery-containing WEEE on a dataset of images captured at 120kV and 100mA and captured at 60kV and 40mA, with three operating points given for both datasets.

By evaluating the ROC-curve, a favourable operating point can be selected in function of the objective of the application. Three possible operating points are shown for both datasets in Figure 4. Operating point 1 shows the highest reached TPR at an FPR of zero. This can be achieved by setting a high confidence threshold, resulting in a low probability of detecting objects other than batteries and the correct classification of all non-battery-containing devices. However, this setting is highly undesirable as many battery-containing products will also be classified as non-battery-containing, resulting in a low TPR and a substantial amount of undetected batteries. In contrast, operating point 2 shows the lowest reached FPR at a TPR of one, which can be achieved by setting a low confidence threshold. This resulted in the correct classification of all battery-containing devices. However, many devices without a battery will, in this case, be classified as battery-containing, resulting in a high number of false detections and many devices needing to be opened even though no battery is inside. The Youden index (operating point 3) is a method to make a trade-off between both the TPR and FPR and determine an optimal operating point. It is defined as the maximal distance between the ROC-curve and the random classification line or:

$$\text{Youden index} = \text{TPR} - \text{FPR} + 1 \tag{3}$$

Using the Youden index, this trade-off was determined at a TPR of 91% and an FPR of 6% for high-intensity X-Ray images and a TPR of 91% and FPR of 21% for low-intensity images. This difference in FPR indicates the rationale for using high intensity X-Ray images for distinguishing between battery and non-battery-containing

devices. However, a larger dataset of device X-Ray images without a battery is required to validate this statement. Training on a larger dataset of images could also further improve the classification performance. Although, the Youden index provides a trade-off between the TPR and FPR, a working point towards a TPR of 1 is most relevant for the application of battery separation to prevent undetected batteries to be processed along with the other materials. However, reaching a TPR of 1 is unrealistic in practice and the cost of dismantling non-battery-containing devices (a high FPR) must also be considered. Therefore, future work will need to determine the current rate of TPR and FPR for battery-containing devices sorted by factory workers to define the minimal requirements for the acceptance by legislation and personal acceptance for industrial implementation of the envisaged sorting system using XRT. At the same time, it will be relevant to quantify the economic and environmental impact of, on the one hand, opening a device for battery removal that does not contain a battery and, on the other hand, not sorting a battery containing device to determine an optimal working point.

### *3.2. Battery detection for battery dismantling*

The same weights were used to evaluate battery detection. The evaluation was performed in regard to the number of correctly located batteries instead of the number of correctly classified battery and non-battery-containing devices, as described in the previous section. For detection, a true positive is defined by a correct battery detection, a false positive is defined by the incorrect detection of an object other than a battery, and a false negative is defined by not detecting a battery annotation. As the ability to locate an object is evaluated, the ability to not detect an object, which was determined by calculating the FPR (2) for classification, cannot be calculated to evaluate detection. Instead, the precision-recall curve (PR-curve) was calculated. Recall is the same evaluation metric as TPR (1), whereas precision defines the number of batteries detected correctly over the total number of detections, as described in equation 4.

$$\text{Precision} = \frac{\text{True positives}}{\text{True positives} + \text{False positives}} \tag{4}$$

Precision is considered to be an important metric because the additional detection of many false positives would result in more time required to treat a device. Recall is still considered of great importance, as any undetected battery would be shredded without additional operations. For this evaluation, a positive condition was defined as an intersection-of-union (IoU) of at least 50% between the proposed bounding box and the ground truth bounding box of the battery annotation. The resulting PR-curve calculation is shown in Figure 5.

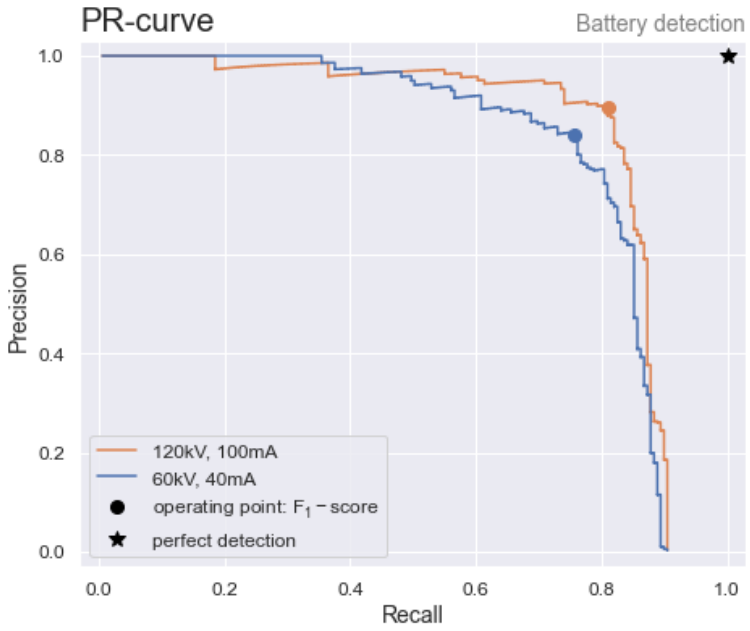


Figure 5. PR-curve of detecting batteries on X-Ray images on a validation set of X-Ray images of WEEE.

The $F_1$ score was calculated at every confidence threshold and the maximal $F_1$ score was marked to determine an optimal operating point. Since the Youden index is an evaluation metric for the ROC-curve, the $F_1$ score is used as an evaluation metric for the PR curve using equation 5.

$$F_1 = 2 * \frac{precision \cdot recall}{precision + recall} \tag{5}$$

Using the $F_1$ score, an optimal operating point is found for the dataset of high-intensity XRT images at a precision of 89% and a recall of 81%. This is expected to be due to the ability to better distinguish different batteries from each other on the same image, as more structural features become visible. However, the same maximal recall of 90% is found for both datasets, whereas a recall or TPR of 100% is demonstrated for classifying battery-containing from non-battery-containing devices, as shown in Figure 4. This is expected to be partially in consequence of multiple overlapping batteries preventing individual detections, for example in battery packs, flashlights, and power tools, as shown in Figure 6a. Based on the presented results, it can be concluded that it will be essential for industrial applications to increase the recall of the detections of batteries in order to ensure that all batteries will be correctly detected, for example, for the purpose of automated dismantling. However, considering the relatively small dataset, the detection of batteries using deep learning architectures is demonstrated to encompass great potential.

### *3.3. Battery recognition for sorting*

The weights trained to recognize the six classes of battery-structures are used to evaluate battery recognition. The same methodology used to evaluate battery detection in the previous section is used here with the addition of the correct prediction of the battery-structure, as an extra requirement for a positive condition. The maximal $F_1$ score (which was portrayed by the $F_1$ score operating point in Figure 5) is shown for every class in Table 2. The

average $F_1$ score is given to evaluate the overall performance and the precision and recall values at the $F_1$ score are given as a reference.

Table 2. $F_1$ score and average $F_1$ score for evaluating the recognition of different battery-structures on the dataset of X-Ray images captured at 120kV and 100µA and captured at 60kV and 40µA. The F1 score for battery detection (Figure 5) and the precision and recall value at the F1 score operating point are given as a reference for comparison.

| | 60kV, 40mA | | | 120kV, 100mA | | | |
|---|---|---|---|---|---|---|---|
| | F1 score | Precision | Recall | F1 score | Precision | Recall | |
| **Battery** | 0.80 | 0.84 | 0.76 | 0.85 | 0.89 | 0.81 | *Detection (one class)* |
| **Cylindrical alkaline** | 0.78 | 0.75 | 0.81 | 0.88 | 0.98 | 0.79 | *Recognition (six classes)* |
| **Cylindrical NiMH/NiCd** | 0.52 | 0.46 | 0.59 | 0.77 | 0.84 | 0.71 | |
| **Button cell** | 0.58 | 0.70 | 0.50 | 0.69 | 0.79 | 0.61 | |
| **Pouch LIB** | 0.78 | 0.88 | 0.70 | 0.86 | 0.82 | 0.90 | |
| **Cylindrical zinc-carbon** | 0.74 | 1.00 | 0.59 | 0.91 | 0.94 | 0.88 | |
| **Cylindrical LIB** | 0.53 | 0.67 | 0.44 | 0.71 | 0.75 | 0.67 | |
| **Average score** | 0.66 | 0.74 | 0.61 | 0.80 | 0.85 | 0.76 | |

With an average $F_1$ score of 80% for battery recognition on the high-intensity XRT image dataset and only 66% on the low intensity dataset, a substantial difference in recognition accuracy can be observed. As hypothesised, the increased amount of visible structural features caused by increased material penetration allow different classes of batteries to be better distinguished. For example, NiMH/NiCd batteries and cylindrical LIBs consist of dense material and are generally used in devices that contain other dense components such as power tools, handheld vacuum cleaners, electric razors, and electric toothbrushes (example on Figure 6b). Pouch LIBs consist of less dense materials but are also used in compact devices that generally contain components that overlap on the XRT image, such as cell-phones, cameras, and other portable electronics (example on Figure 6c). Despite the irregular shape of pouch LIBs, together with alkaline and zinc-carbon batteries, the $F_1$ score is the highest for the recognition of these battery types. This demonstrates that the adopted methodology is suited for the recognition of both regular and irregular shaped batteries, which is a great advantage compared to state-of-the-art battery sorting systems and which is of great value to increase the efficiency of the current battery sorting process.

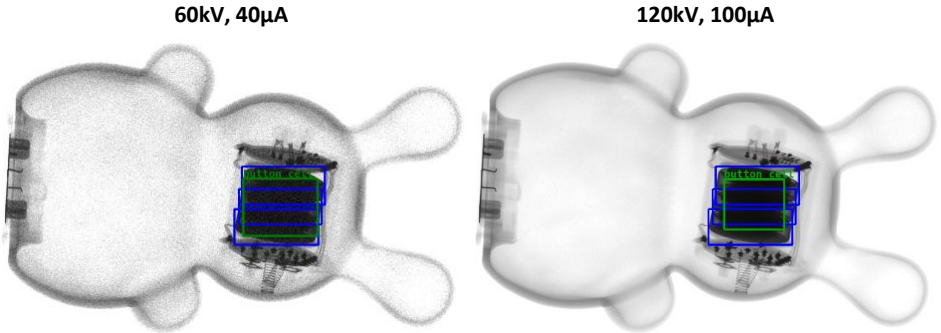


(a) Toy figure with button cells. Three button cells are detected as one button cell on both images.

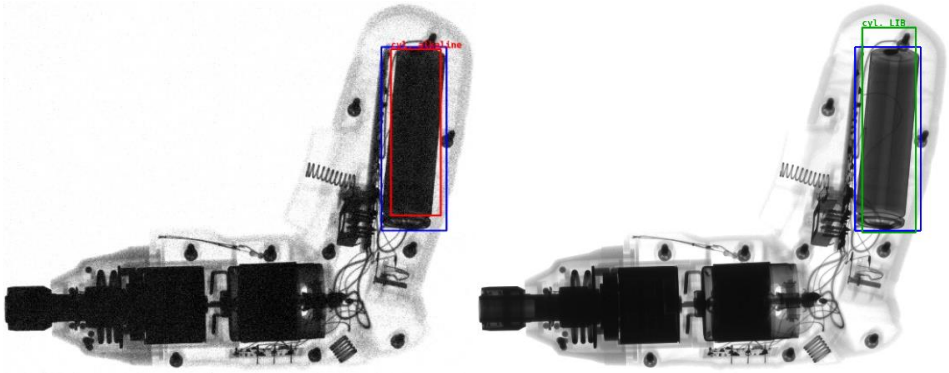


(b) Drill with cylindrical LIB. The battery-structure is recognized false as an alkaline battery on the low-intensity X-Ray image.

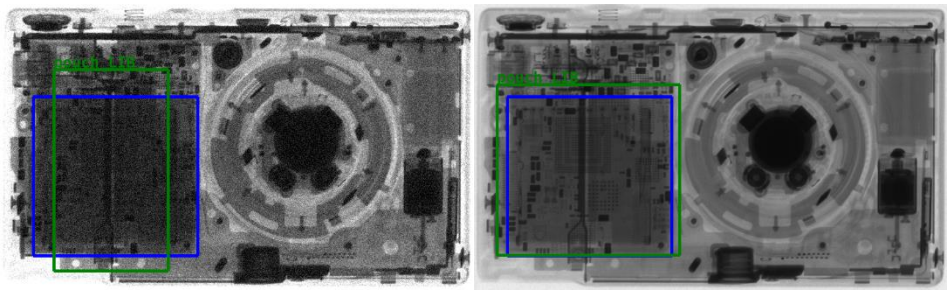


(c) Camera with pouch LIB which is recognized on both images even though other components overlap the battery.

Figure 6. Examples of battery-structure recognitions on the 60kV, 40µA image datasets and the 120kV, 100µA dataset with true positives shown in green, false positives shown in red, and annotations shown in blue.

Overall, the results for recognition demonstrate the feasibility of using this technique to sort batteries based on their technologies. The substantial increase in the $F_1$ score between the X-Ray Image dataset with low and high-intensity settings also demonstrated the added value of using an X-Ray machine with a power setting of 120kV-100µA. Nevertheless, as the dataset of products was divided into a relatively small number of devices for each class, significant improvements in detection and recognition are expected to be achievable with a larger product dataset. For this study, the Youden index and $F_1$ score were used to determine an optimal operating point. In future work, this operating point can also be determined by assessing the impact or consequence of false positive and false negative detections, such as the cost of unnecessary actions that are performed when a device is incorrectly sorted as battery-containing or the consequence when an incorrect battery-structure is recognised and a battery ends up in the wrong fraction causing the mixing of different battery chemistries.

## 4. Conclusions and future work

The labour intensity of sorting battery-containing devices and of manually dismantling and sorting the removed batteries results in high treatment costs. As the share of products containing battery packs and pouch cell batteries is expected to increase, there is a prevalent need for innovative battery sorting and dismantling strategies. Therefore, the potential of implementing the classification of battery-containing devices, the detection of battery locations, and the recognition of battery-structures on X-Ray images of WEEE to allow automated sorting and separation is investigated. X-Ray images were captured to generate a dataset of 532 images of electronic devices at two X-ray imaging settings with the aim of evaluating the hardware design required for industrial implementation.

Results obtained with the limited dataset are promising and showed the best results with the high-intensity X-ray images for all applications. With these images, an operation point was found to classify battery-containing devices from non-battery-containing devices at a true positive rate of 91% and a false positive rate of 6%. Additionally, to detect individual battery locations, 89% accuracy and 81% recovery were demonstrated. Finally, an average precision of 85% and an average recall of 76% were demonstrated to distinguish between battery technologies. Hence, the presented results demonstrate that deep learning architectures for battery detection and recognition in XRT images are a promising strategy for the cost-efficient detection and recognition of batteries in WEEE.

Even though these findings are promising, future work is required to determine whether XRT imaging for the sorting and dismantling of batteries from WEEE is economically viable on an industrial scale. Nevertheless, the results provide clear guidelines and methods for the further development of such systems. First of all, the accuracy of the automated sorting of battery-containing devices should be at least be similar to manual sorting accuracies currently achieved. Otherwise, it will be necessary to consider a man-machine collaboration in the evaluation of the economic viability. Second, systems that make use of the detected battery locations to (semi-) automatically sort battery containing products and dismantle batteries are currently under development. The ability of these systems to safely sort and remove batteries will need to be ensured, and the costs of sorting and dismantling will need to be taken into account when determining the economic viability of XRT battery detection as part of the entire system. Third, the advantages of recognizing the battery type for safer manual dismantling, to enable future automated dismantling, or to enable destructive processing that is only viable for certain battery types, will need to be further investigated.

Therefore, the costs of an XRT imaging setup in combination with automated sorting and dismantling systems will be contrasted with the economic advantages such a system would entail. A larger dataset of representative images will also be captured by making us of an industrial X-Ray line scanner that will be built based on the settings determined during this study and a larger selection of deep learning architectures will be investigated and tested. In this dataset, the share of non-battery-containing devices will be increased to obtain more insights on the ability to distinguish non-battery-containing from battery-containing devices. To increase the detection accuracies required to eliminate the need for manual verification, the use of dual-energy and multispectral X-Ray imaging will also be investigated. Finally, the benefits of combining information from XRT images with information from other sensors, such as the identified model or category from text detection and recognition will also be investigated.

## References


Akcay, S., Kundegorski, M. E., Willcocks, C. G., & Breckon, T. P. (2018). Using Deep Convolutional Neural Network Architectures for Object Classification and Detection Within X-Ray Baggage Security Imagery. *IEEE Transactions on Information Forensics and Security*, *13*(9), 2203–2215. https://doi.org/10.1109/TIFS.2018.2812196

*AMP Cortex™*. (2020). AMP Robotics. https://www.amprobotics.com/amp-cortex

Bebat. (2020). *Sorting*. https://www.bebat.be/en/sorting

Bigum, M., Damgaard, A., Scheutz, C., & Christensen, T. H. (2017). Environmental impacts and resource losses of incinerating misplaced household special wastes (WEEE, batteries, ink cartridges and cables). *Resources, Conservation and Recycling*, *122*, 251–260. https://doi.org/10.1016/j.resconrec.2017.02.013

Bobulski, J., & Kubanek, M. (2019). Waste Classification System Using Image Processing and Convolutional Neural Networks. In I. Rojas, G. Joya, & A. Catala (Eds.), *Advances in Computational Intelligence* (pp. 350–361). Springer International Publishing. https://doi.org/10.1007/978-3-030-20518-8_30

Chen, H., & Shen, J. (2017). A degradation-based sorting method for lithium-ion battery reuse. *PLoS ONE*, *12*(10). https://doi.org/10.1371/journal.pone.0185922

Cheret, D., & Santen, S. (2007). *Battery recycling* (United States Patent No. US7169206B2). https://patents.google.com/patent/US7169206B2/en

*COMMUNICATION FROM THE COMMISSION TO THE EUROPEAN PARLIAMENT, THE COUNCIL, THE EUROPEAN ECONOMIC AND SOCIAL COMMITTEE AND THE COMMITTEE OF THE REGIONS A new Circular Economy Action Plan For a cleaner and more competitive Europe* (COM/2020/98 final). (2020). European Commission. https://eur-lex.europa.eu/legal-content/EN/TXT/?qid=1583933814386&uri=COM:2020:98:FIN

*COMMUNICATION FROM THE COMMISSION TO THE EUROPEAN PARLIAMENT, THE COUNCIL, THE EUROPEAN ECONOMIC AND SOCIAL COMMITTEE AND THE COMMITTEE OF THE REGIONS Closing the loop—An EU action plan for the Circular Economy* (COM/2017/0173 final). (2015). https://eur-lex.europa.eu/legal-content/EN/TXT/?uri=CELEX:52015DC0614

*Consolidated text: Directive 2012/19/EU of the European Parliament and of the Council of 4 July 2012 on waste electrical and electronic equipment (WEEE) (recast) (Text with EEA relevance)* (No. 02012L0019). (2018). The European Parliament and the Council of the European Union. https://eur-lex.europa.eu/legal-content/EN/TXT/?uri=CELEX%3A02012L0019-20180704

Danish Technological Institute (DTI), Refind, & Stena. (2018, March 23). *New Robot System Extracts Dangerous and Valuable Items From Waste Using Artificial Intelligence*. https://www.dti.dk/new-robot-system-extracts-dangerous-and-valuable-items-from-waste-using-artificial-intelligence/39554

Deloitte Sustainability, British Geological Survey, Bureau de Recherches Geologiques et Minieres, & Netherlands Organisation for Applied Scientific Research. (2017). *Study on the review of the list of critical raw materials—Criticality Assessment*. Publications Office of the European Union. https://op.europa.eu/en/publication-detail/-/publication/08fdab5f-9766-11e7-b92d-01aa75ed71a1/language-en

Directive 2012/19/EU of the European Parliament and of the Council of 4 July 2012 on waste electrical and electronic equipment (WEEE), 32012L0019, CONSIL, EP, OJ L 24.7.2012 (2012). http://data.europa.eu/eli/dir/2012/19/oj/eng

*Directive (EU) 2018/849 of the European Parliament and of the Council of 30 May 2018 amending Directives 2000/53/EC on end-of-life vehicles, 2006/66/EC on batteries and accumulators and waste batteries and accumulators, and 2012/19/EU on waste electrical and electronic equipment (Text with EEA relevance)* (PE/9/2018/REV/1; Vol. 150). (2018). The European Parliament and the Council of the European Union. http://data.europa.eu/eli/dir/2018/849/oj/eng

*Factsheet: An ambitious EU circular economy package*. (2015). [Factsheet]. European Commission. https://ec.europa.eu/commission/publications/ambitious-eu-circular-economy-package_en

Fu, C.-Y., Liu, W., Ranga, A., Tyagi, A., & Berg, A. C. (2017). DSSD: Deconvolutional Single Shot Detector. *ArXiv:1701.06659 [Cs]*. http://arxiv.org/abs/1701.06659

Gratz, E., Sa, Q., Apelian, D., & Wang, Y. (2014). A closed loop process for recycling spent lithium ion batteries. *Journal of Power Sources*, *262*, 255–262. https://doi.org/10.1016/j.jpowsour.2014.03.126

Hedegor, E., Oliver, R., & Sawahara, S. (2004). *Battery tester and sorting apparatus* (United States Patent No. US20040155626A1). https://patents.google.com/patent/US20040155626A1/en

Herrmann, C., Raatz, A., Mennenga, M., Schmitt, J., & Andrew, S. (2012). Assessment of Automation Potentials for the Disassembly of Automotive Lithium Ion Battery Systems. In D. A. Dornfeld & B. S. Linke (Eds.), *Leveraging Technology for a Sustainable World* (pp. 149–154). Springer. https://doi.org/10.1007/978-3-642-29069-5_26

InnospeXion. (2020). *Garbage & Waste Sorting X-ray Inspection*. https://innospexion.dk/garbage-waste-sorting-x-ray-inspection-product-process-control-innospexion/

Jiao, L., Zhang, F., Liu, F., Yang, S., Li, L., Feng, Z., & Qu, R. (2019). A Survey of Deep Learning-based Object Detection. *IEEE Access*, *7*, 128837–128868. https://doi.org/10.1109/ACCESS.2019.2939201

Karbasi, H., Sanderson, A., Sharifi, A., & Pop, C. (2018). Robotic Sorting of Used Button Cell Batteries: Utilizing Deep Learning. *2018 IEEE Conference on Technologies for Sustainability (SusTech)*, 1–6. https://doi.org/10.1109/SusTech.2018.8671351

Li, J., Shi, P., Wang, Z., Chen, Y., & Chang, C.-C. (2009). A combined recovery process of metals in spent lithium-ion batteries. *Chemosphere*, *77*(8), 1132–1136. https://doi.org/10.1016/j.chemosphere.2009.08.040

Lin, T.-Y., Goyal, P., Girshick, R., He, K., & Dollár, P. (2017). Focal Loss for Dense Object Detection. *ArXiv:1708.02002 [Cs]*. http://arxiv.org/abs/1708.02002

Lisbona, D., & Snee, T. (2011). A review of hazards associated with primary lithium and lithium-ion batteries. *Process Safety and Environmental Protection*, *89*(6), 434–442. https://doi.org/10.1016/j.psep.2011.06.022

Liu, W., Anguelov, D., Erhan, D., Szegedy, C., Reed, S., Fu, C.-Y., & Berg, A. C. (2016). SSD: Single Shot MultiBox Detector. *ArXiv:1512.02325 [Cs]*, *9905*, 21–37. https://doi.org/10.1007/978-3-319-46448-0_2

Lukka, T. J., Tossavainen, T., Kujala, J. V., & Raiko, T. (2014). *ZenRobotics Recycler—Robotic Sorting using Machine Learning*. Undefined. /paper/ZenRobotics-Recycler-Robotic-Sorting-using-Machine-Lukka-Tossavainen/6d7caa11da0ff2dd1f2c1a8740c5b0858da636f1

Mallant, J. P., Schumann, R., Moritz, T., & Justus, H. C. (1996). *Optical sorting system for a color sorting machine and process* (United States Patent No. US5579921A). https://patents.google.com/patent/US5579921A/en

Mathieux, F., Ardente, F., Bobba, S., Nuss, P., Blengini, G. A., Alves Dias, P., Blagoeva, D., Torres de Matos, C., Wittmer, D., Pavel, C., & Šolar, S. V. (2017). *Critical raw materials and the circular economy JRC science for policy report: Background report* (p. 50). Publications Office of the European Union.

*Max-AI*. (2020). Max-AI. https://www.max-ai.com/autonomous-qc/

Montagner, F., Kaftandjian, V., Duvauchelle, P., Pedoussaut, N., & Bourely, A. (2014, October). Dual Energy Radioscopy Applied to Waste Sorting. *European Conference on Non Destructive Testing*. https://hal.archives-ouvertes.fr/hal-01282258

*Ontwerp van decreet betreffende maatwerk bij collectieve inschakeling*. (2013). (Flemish Department of Work and Social Economy. http://k00316.staging.cloud.kanooh.be/sites/default/files/Maatwerkdecreet%207%20juni%202013.pdf

Ophoff, T. (2018). *Lightnet: Building Blocks to Recreate Darknet Networks in Pytorch*. https://gitlab.com/EAVISE/lightnet

Peeters, J. R., Vanegas, P., Dewulf, W., & Duflou, J. R. (2016). *Economic and environmental evaluation of design for active disassembly | Elsevier Enhanced Reader*. *140*, 1182–1193. https://doi.org/10.1016/j.jclepro.2016.10.043

*Proposal for a DIRECTIVE OF THE EUROPEAN PARLIAMENT AND OF THE COUNCIL amending Directive 2008/98/EC on waste* (COM/2015/0595 final-2015/0275 (COD)). (2015). The European Parliament and the Council of the European Union. https://eur-lex.europa.eu/legal-content/EN/TXT/?uri=CELEX:52015PC0595

Rajpurkar, P., Irvin, J., Zhu, K., Yang, B., Mehta, H., Duan, T., Ding, D., Bagul, A., Langlotz, C., Shpanskaya, K., Lungren, M. P., & Ng, A. Y. (2017). CheXNet: Radiologist-Level Pneumonia Detection on Chest X-Rays with Deep Learning. *ArXiv:1711.05225 [Cs, Stat]*. http://arxiv.org/abs/1711.05225

Recupel. (2019). *Innovatief en meer circulair*. https://recupel.prezly.com/innovatief-en-meer-circulair

Redmon, J., & Farhadi, A. (2016). YOLO9000: Better, Faster, Stronger. *ArXiv:1612.08242 [Cs]*. http://arxiv.org/abs/1612.08242

Redux. (2020). Portable & Consumer Batteries. *REDUX – Smart Battery Recycling*. https://www.redux-recycling.com/en/services/portable-consumer-batteries/

Refind. (2019). *Optical Battery Sorter 500*. https://www.refind.se/optical-battery-sorter-500

Ren, S., He, K., Girshick, R., & Sun, J. (2016). Faster R-CNN: Towards Real-Time Object Detection with Region Proposal Networks. *ArXiv:1506.01497 [Cs]*. http://arxiv.org/abs/1506.01497

Russakovsky, O., Deng, J., Su, H., Krause, J., Satheesh, S., Ma, S., Huang, Z., Karpathy, A., Khosla, A., Bernstein, M., Berg, A. C., & Fei-Fei, L. (2015). ImageNet Large Scale Visual Recognition Challenge. *International Journal of Computer Vision*, *115*(3), 211–252. https://doi.org/10.1007/s11263-015-0816-y

Sonoc, A., Jeswiet, J., & Soo, V. K. (2015). Opportunities to Improve Recycling of Automotive Lithium Ion Batteries. *Procedia CIRP*, *29*, 752–757. https://doi.org/10.1016/j.procir.2015.02.039

Takezawa, T., Uemoto, M., & Itoh, K. (2015). Combination of X-ray transmission and eddy-current testing for the closed-loop recycling of aluminum alloys. *Journal of Material Cycles and Waste Management*, *17*(1), 84–90. https://doi.org/10.1007/s10163-013-0228-4

Umicore. (2020, May 4). *Indium*. https://www.umicore.com/en/about/elements/indium/

Wang, X., Gaustad, G., & Babbitt, C. W. (2016). Targeting high value metals in lithium-ion battery recycling via shredding and size-based separation. *Waste Management*, *51*, 204–213. https://doi.org/10.1016/j.wasman.2015.10.026

Yamaji, Y., Dodbiba, G., Matsuo, S., Okaya, K., Shibayama, A., & Fujita, T. (2011). A Novel Flow Sheet for Processing of Used Lithium-ion Batteries for Recycling. *Resources Processing*, *58*(1), 9–13. https://doi.org/10.4144/rpsj.58.9